ACS APPLIED MATERIALS & INTERFACES

Research Article

www.acsami.org

A Switch of the Oxidation State of Graphene Oxide on a Surface Plasmon Resonance Chip

Tianyu Xue, Xiaoqiang Cui,* Jianli Chen, Chang Liu, Qiyu Wang, Haitao Wang, and Weitao Zheng*

Key Laboratory of Automobile Materials of MOE and State Key Laboratory of Superhard Materials, Department of Materials Science, Jilin University, Changchun 130012, People's Republic of China

Supporting Information

ABSTRACT: Controlling the assembly and manipulating the oxidation state of graphene nanosheets on surfaces are of essential importance for application of graphene-related optical and biosensing devices. In this study, we assemble a graphene oxide (GO) film on a surface plasmon resonance chip surface and then convert it to reduced graphene by an in situ electrochemical method. The mechanism and application of surface-enhanced Raman spectroscopy and DNA sensing from graphene-based substrates are investigated. The average thickness and dielectric constant of GO are varied significantly with the switch of its oxidation state. Electrochemical reduction decreases the distance between carbon atoms and the gold surface by removing the spacer of oxygen functional groups. The electromagnetic field of the graphene surface is therefore enhanced, resulting in an enhancement of the Raman signal. A p doping of electrochemically reduced GO (ERGO) that occurred from changes in the graphene electronic structure through interaction between gold and ERGO is also observed during electrochemical reduction. The GO and ERGO substrates perform different interaction abilities with single- and double-stranded DNA. This work may be valuable for graphene-related research works on optoelectronics and biosensors.

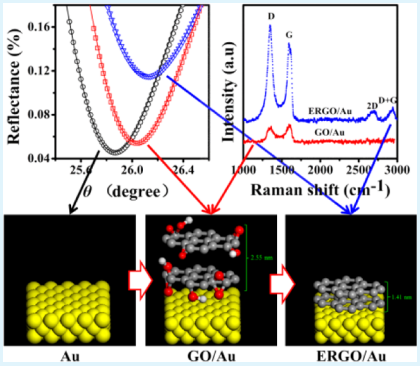

KEYWORDS: *graphene oxide, surface plasmon resonance, SERS, electrochemical reduction, DNA binding*

1. INTRODUCTION

Graphene, a single layer of carbon atoms in a closely packed honeycomb two-dimensional structure, has attracted extensive interest since its discovery in 2004.[1−3] It promises exciting application potentials in various fields, such as supercapacitors,[4,5] nanocomposite materials,[6,7] electronic devices,[8] cell images,[9] and sensors.[10,11] There are many approaches to the preparation of graphene including mechanical exfoliation,[1] chemical vapor deposition,[12] epitaxial growth,[13] creation of colloidal suspensions,[9] and chemical/electrochemical reduction of graphene oxide (GO).[14,15] The synthesis route from GO is considered to be the most economical way to mass produce graphene. However, the excessive reducing reagents employed in chemical reduction may contaminate the resulting materials and cannot fully remove the oxygenic functional groups. An electrochemical method is an effective tool to modify the electronic state by adjusting the external power source to change the Fermi energy level of electrode surfaces.[16,17] Interest among chemists and researchers from multidisciplines has increasingly been attracted to using GO as a precursor of graphene.[16,18] GO can be well dispersed in aqueous solution and has been widely used in the preparation of graphene-based nanocomposites because of its abundant oxygen-containing functional groups.[18,19] The recent discoveries of graphene-based plasmonic phenomena have shown great potential applications in optoelectronics, plasmonics, and transformation optics, in which the controlled assembly of graphene is in high demand.[20,21] Although the graphene sheets can be processed into large-area films via wet-processing techniques such as spin coating and filtration,[22,23] it is still difficult to control the thickness and to convert the assembled GO into reduced graphene without losing the quality of the GO film. Seeking an approach to controlling the assembly and oxidation state of the GO film is of essential importance for various applications in electronic devices and biosensors.[24]

We propose a facile method to assemble the GO film on a surface plasmon resonance (SPR) chip surface using the strong metal−carbon coupling between GO and the gold (Au) surface.[25] The assembled GO film is converted into reduced graphene by an in situ electrochemical method without any loss of the film quality. SPR spectroscopy is a very powerful tool to detect small changes of the refractive index occurring on the noble metal surface.[26,27] This technology has been widely used for the detection of protein, DNA, conductive polymers, and other materials.[21] Compared with conventional techniques of thermogravimetric analysis,[28] atomic force microscopy (AFM),[29] UV−visible absorption,[30] X-ray photoelectron spectroscopy (XPS),[31] and Raman spectroscopy,[32] SPR not only presents a real-time monitoring GO assembly but also provides information on the film thickness and dielectric constant

Received: December 7, 2012
Accepted: March 2, 2013
Published: March 2, 2013

variations of GO when it is reduced. In this study, we characterize the thickness and dielectric constants of assembled GO and electrochemically reduced GO (ERGO) by SPR spectroscopy, AFM, electrochemical impedance spectroscopy (EIS), XPS, and contact angle. Interestingly, ERGO on Au exhibits significant enhancement for the Raman signal. This enhancement is ascribed to (1) a decrease of the distance between carbon atoms and the Au surface by removal of the spacer of oxygen functional groups and (2) a p doping from changes in the ERGO electronic structure by interaction between Au and ERGO during electrochemical reduction. The results also show that GO and ERGO substrates perform different interaction abilities with single- and double-stranded DNA. This work should be valuable for graphene-related research work on optics and biosensors.

2. EXPERIMENT

2.1. Preparation of GO. GO is synthesized by a modified Hummer's method.[33] Typically, 2.0 g of graphite powder is dissolved in a mixture of concentrated H_2SO_4 (98 wt %, 67.5 mL) and $NaNO_3$ (1.5 g) under stirring. $KMnO_4$ is gradually added into the reaction container under stirring in an ice bath for 2 h. The reaction is kept for 5 days at room temperature with modest stirring. The graphite oxide dispersion is treated ultrasonically (at 40 Hz with power of 320 W) for about 2 h to ensure that most graphite oxide is exfoliated into single-layer GO. The supernatant liquor is collected for the next procedure.

2.2. SPR Measurement. SPR spectrometry is carried out using a TR2005 spectrometer (RES-TEC resonant sensor technology, Germany). The setup is based on the conventional Kretchmann configuration including a He−Ne laser of wavelength λ = 632.8 nm, which is coupled to the system via a high-refractive-index prism, LAFSN9 glass ε = 3.40.[34] The Au-coated sensor chip mounted with a homemade electrochemical flow cell is attached to the prism base with high-index-matching oil. The reflected light is detected by a photodiode.[35,36]

During the experiments, water is injected over the Au surface. The kinetic measurements by SPR are conducted for at least 12 h using a kinetic method (mode tracking). The sensor chip surface is then rinsed with water and dried under a flow of dinitrogen. Cyclic voltammetry experiments are carried out in phosphate-buffered saline (PBS; pH 7.4). EIS is performed under an oscillation potential of 0.23 V over a frequency range of 10−0.1 kHz. The amplitude of the alternate voltage is 5 mV. EIS is performed in a mixture of 5 mM $Fe(CN)_6^{3-}/Fe(CN)_6^{4-}$ (1:1) with 0.1 M KCl on a CHI650D electrochemical workstation (Shanghai, Chenhua Co., China). A three-electrode cell is used with the Au film as the working electrode, a AgCl electrode as the reference electrode, and a platinum electrode as the counter electrode. All experiments are done at room temperature.

2.3. Instruments. Transmission electron microscopy (TEM) images are taken with a Hitachi H-8100 IV instrument operating at 200 kV (FEI Co., USA). AFM images are obtained with ScanAsyst in air mode on Bruker Dimension Icon scanning probe microscope (Bruker Co., Germany). XPS images are acquired with an ESCALAB-250 instrument [performed with a monochromatic Al Kα (1486.6 eV) radiation source and a hemisphere detector with an energy resolution of 0.1 eV]. Contact-angle measurements are made using ultrapure water at room temperature using a contact-angle goniometer and drop-shape analysis system DSA30 (Krüss Co., Germany). The drops are placed on the surface, and high-contrast images are captured after 10 s. Raman spectra of Rhodamine 6G (R6G) and crystal violet (CV) molecules are obtained from the three different states on Au and indium−tin oxide (ITO) substrates using excitation wavelengths 514 and 633 nm under normal incident light. The Raman spectra using excitation wavelength 514 nm are detected with a Renishaw 1000 microspectrometer connected to a Leica microscope with an objective lens of 50× (NA = 0.5). The Raman spectra using excitation wavelength 633 nm are measured with a Jobin Yvon/Horiba LabRam ARAMIS Raman spectrometer. A droplet of an ethanol solution of R6G (or CV) dye (10^{-5} M, 5 μL) is added in an O-ring rubber (the diameter is 8 mm) on ERGO/Au, GO/Au, and Au substrates. Their Raman spectra are measured after the evaporation of ethanol. The typical accumulation time used in this study is 10 s.

3. RESULTS AND DISCUSSION

3.1. Characterization of GO Nanosheets. Water-soluble GO nanosheets prepared according to a modified Hummers' method are characterized by TEM and AFM (as shown in Figure 1). The TEM image shows that GO consists of well-

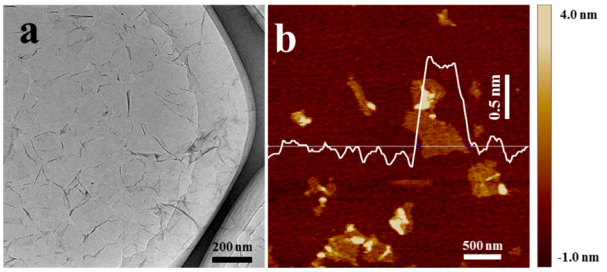

Figure 1. TEM image of GO (a) and AFM image of GO on mica (b).

dispersed wrinkled and folded flakes. The thickness of the GO sheets, obtained by analysis of the AFM cross-sectional profile, is about 1.1 nm, which is consistent with previous reports, suggesting the single-sheet nature of GO in this work.[37]

3.2. Assembly and in Situ Electrochemical Reduction of GO on a Au Sensor Chip. Considering the strong metal−carbon coupling between GO and the Au surface, two-dimensional GO nanosheets are expected to self-assemble on a flat Au surface.[25] The assembly process of GO on a Au sensor chip is monitored by a SPR technique (Figure 2).[38] The SPR

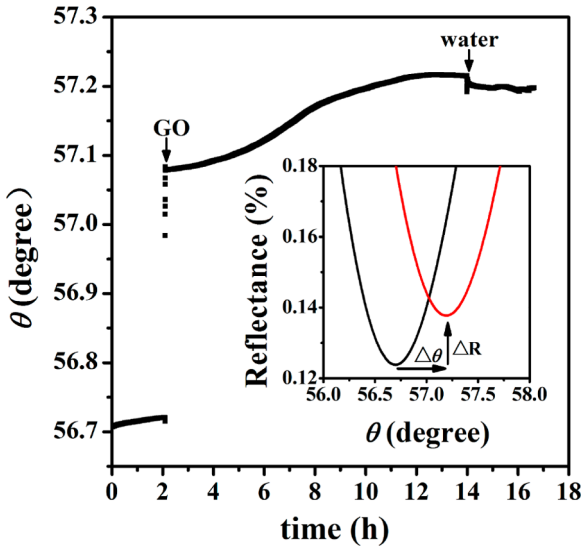

Figure 2. Real-time characterization of GO assembly on the Au surface by SPR. The inset shows the SPR angular reflectivity spectra before and after GO adsorption.

baseline is stable after 2 h of injection of GO aqueous solution. The sharp increase of the SPR response is attributed to the change of the refractive index.[39] The adsorption rate is low in the first 3 h, indicating that adsorption of GO on the Au surface is under mass-transport limitation.[40] There is a mass uptake signaled by a monotonic increase of the resonance angle, which

dx.doi.org/10.1021/am400481t | ACS Appl. Mater. Interfaces 2013, 5, 2096−2103

saturates after 12 h at a resonance angle shift of around 0.50°. Deionized water is then injected to wash away nonabsorbed GO. This kinetic curve of the GO assembly is in accordance with the self-assembly of polyelectrolyte macromolecules on charged surfaces.[41] The inset in Figure 2 shows the revolution of the SPR curve in both resonance angle and reflectivity when a thin layer of GO is assembled on a Au sensor chip surface. An increase of the SPR angle confirms the adsorption of GO on the Au sensor chip. A decrease of the reflection loss indicates that GO belongs to the absorbing dielectric medium.[42]

An electrochemical method is an effective tool to modify electronic states by adjusting the external power source to change the Fermi energy level of the electrode material surface. It has been proven to be a simple, fast, efficient, low-cost, and environmentally friendly way to produce graphene.[43,44] We use a cyclic voltammetry technique to electrochemically reduce assembled GO nanosheets on the Au film. As shown in Figure 3, GO is reduced at a starting potential of −0.8 V with a current

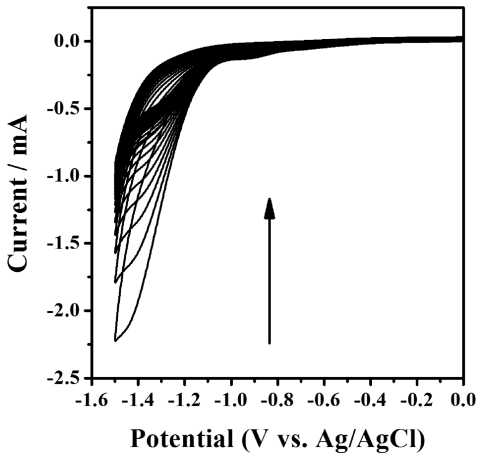

Figure 3. In situ electrochemical reduction of GO on the Au surface by cyclic voltammetry in PBS (pH 7.4) saturated with dinitrogen gas at a scan rate of 50 mV/s.

peak at −1.4 V, which is ascribed to the reduction of oxygen groups of −OH, −COOH, and epoxides.[16,45] The reduction current begins to drop exceptionally in the second cyclic voltammetry scanning cycle and continues to decrease until it has disappeared. This electrochemical behavior is similar to a previous report of the reduction of GO sheets on glass carbon electrodes.[16,46] The procedure of the assembly and in situ reduction is also investigated by the techniques of EIS[17,47] and contact angle.[37] As shown in Figure S1 in the Supporting Information (SI), the diameter of the semicircle corresponding to the electron-transfer resistance (R_{ct}) dramatically increases when GO is modified on the Au surface.[48] This clearly indicates that modification of GO on the electrode surface presents a hindrance effect on the electron-transfer process of $Fe(CN)_6^{3-}$/$Fe(CN)_6^{4-}$. The electrical conductivity is highly improved when GO is electrochemically reduced into ERGO, which is proven by a significant decrease of the charge-transfer resistance value in EIS.[49] GO is highly hydrophilic because the oxidation process creates large numbers of oxygen-containing functional groups of carboxyl, epoxide, and hydroxyl groups on graphene surfaces. As shown in Figure S2a in the SI, GO on the Au film is hydrophilic with a contact angle of 44°. However, its wettability decreases (contact angle 88°) with electrochemical reduction because of removal of the oxygen atoms (Figure S2b in the SI).[37]

The SPR angular reflectivity spectrum is very sensitive to a minor change of the refractive index on the sensor chip surface. We can obtain parameters of average thickness and dielectric constants of the Au film by fitting curves of SPR (Table S1 in the SI). The propagation characteristics of surface plasmons will be altered with changes in both the thickness and oxidation state of the GO film. The color of GO changed from yellow-brown to black after electrochemical reduction, indicating the absorption characteristics of reduced graphene.[50] Consequently, this feature results in a significant shift in the minimum reflectance of SPR curves from GO to ERGO modified surface (as shown in Figure 4). To quantitatively detect the assembly

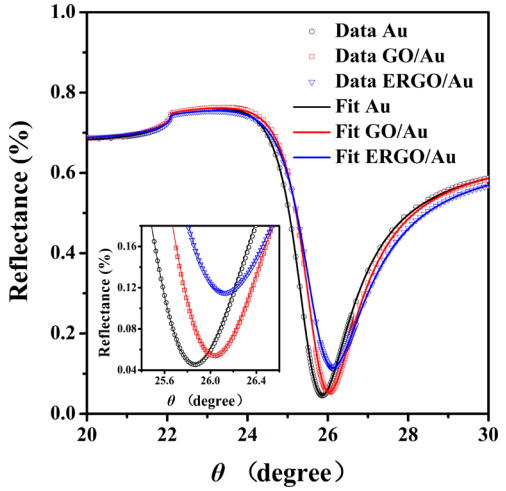

Figure 4. SPR angular reflectivity spectra measured from a bare Au film (black circles), GO/Au (red squares), and ERGO/Au (blue inverted triangles). The solid lines represent simulated reflectivity. The inset shows an enlarged drawing of SPR dips.

and transformation of GO to ERGO, calculations are done using Fresnel's equations. The experimental (data in dots) and theoretical (solid lines) curves of representative SPR spectra from a bare Au film, GO, and ERGO are presented in Figure 4. The average thickness and dielectric constants of the Au film are first obtained from a four-layer system (prism/chromium/Au/air) and summarized in Table S1 in the SI. When the layer of GO/ERGO is involved, a system configuration consisting of five layers (prism/chromium/Au/GO/air) is used for the calculation.

In principle, the width and depth of a SPR spectrum is mainly influenced by the imaginary part of the dielectric constant (ε'') and average thickness (d) in an adsorbed layer.[26] The minimum reflectance increase from 5.36% to 11.48% when GO is electrochemically reduced implies that there may be changes in ε'' and d, which is theoretically calculated based on a five-layer Fresnel equation.[42] The average thickness and dielectric constant of GO/ERGO obtained in our fitting are compared with previous reports in the literature (as shown in Table 1).[51] The discrepancy between the real and imaginary parts of the dielectric constant of GO resulting from the present fit and reference data from the literature is reasonable considering the different oxidation states of the sample. The average thickness of the GO film calculated from SPR is 2.55 nm. This number is close to 2-fold that of the theoretical thickness of a flat monolayer of GO, which is 1.1 nm.[37] This

Table 1. Parameters Obtained from the SPR Fitting Results and a Comparison with Data in References

	d, nm		ε'		ε''	
	fitting results	ref data	fitting results	ref data	fitting results	ref data
GO	2.55	1.1[32]	1.62	2.86[68]	0.01	0.59[68]
ERGO	1.41	0.7[43]	7.41	7.68[69]	2.26	6.89[69]

implies that the assembled GO on the Au surface is about double layer, which is further confirmed by AFM characterization. When GO is in situ reduced on a sensor chip, the average thickness of ERGO is decreased to 1.41 nm. It is worth noting that ε'' is increased more than 200 times from 0.01 to 2.26. Therefore, the significant shift in the minimum reflectance SPR spectrum can be mainly attributed to the increase of ε'' from ERGO.[42] The position of the SPR angle right shifts 0.10° with in situ electrochemical reduction. The reduction of GO to ERGO results in a decrease of d and an increase of ε', which leads to opposing effects on the position of the SPR angle.[52] The SPR angle localization depends both on the thickness (d) and on the real part of the dielectric constant (ε'), but the main parameter governing the position of the SPR angle is variation of the real part of the dielectric constant.[53]

An as-prepared ERGO film on the Au surface is very stable even under ultrasonication in water, ethanol, and acetone. Figure 5 shows the morphological changes of an SPR sensor chip surface during the assembly and in situ electrochemical reduction of GO. The density of the GO sheets has appeared to be very similar in the AFM images before and after electrochemical reduction (Figure 5c,e). This indicates that the loss of GO is not significant after application of a high electrochemical reduction potential. The surface coverage of GO and ERGO is 72.6 ± 7.9% and 69.1 ± 4.5%, respectively. The root-mean-square (RMS) roughness value is increased from 0.48 ± 0.08 to 1.90 ± 0.10 nm when GO is assembled on a Au chip surface. The increase of the surface roughness comes from the random distribution of GO on the bare Au film. With in situ electrochemical reduction, the RMS roughness value of ERGO is decreased to 1.26 ± 0.04 nm. This decrease can be explained by the thickness changes of GO when oxygen-containing functional groups were removed with electrochemical reduction.

Electrochemical reduction of GO to ERGO is analyzed in detail by XPS (as shown in Figure 6).[54] The C 1s XPS spectrum of GO clearly indicates a considerable oxidation with four components that correspond to carbon atoms in functional groups of a nonoxygenated ring (C−C, 284.6 eV), C−O bonds (286.3 eV), carbonyl (C═O, 287.0 eV), and carboxylate (O−C═O, 288.5 eV).[32] The C−O, C═O, and O−C═O peaks in the C 1s spectral area of ERGO accounted for 12.7%, 1.4%, and 1.2%, instead of 14.4%, 25.8%, and 6.8% in the case of GO. These data are interpreted as that most of the oxygen-containing functional groups have been removed after electrochemical reduction.[54,55]

3.3. Raman Characterization. GO and ERGO on Au sensor chips are further characterized by Raman spectroscopy. As shown in Figure 7a, the G peak at ~1591 cm^{-1} is usually assigned to the E_{2g} phonon of C sp^2 atoms, the D peak at ~1347 cm^{-1} is a breathing mode of κ-point phonons of A_{1g} symmetry, and the 2D band at ~2700 cm^{-1} is due to a double-resonance process; the combinational modes D+G band is at 2938 cm^{-1}.[56] The intensity ratio of the D/G band (I_D/I_G) is a measure of the disorder.[57] We calculated I_D/I_G ratios of GO and ERGO on a Au chip surface as 0.89 and 1.24, respectively. The change can be explained by a decrease in the average size

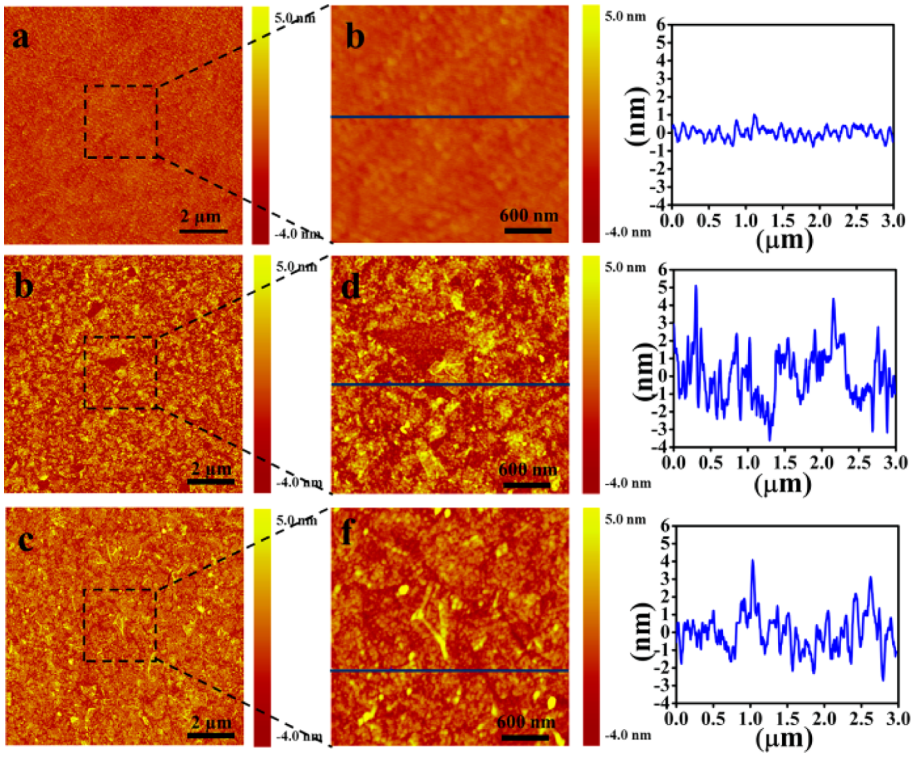

Figure 5. AFM images: (a and b) bare Au film, RMS = 0.48 ± 0.08 nm; (c and d) GO assembled on a Au film, RMS = 1.90 ± 0.10 nm; (e and f) ERGO on a Au film, RMS = 1.26 ± 0.04 nm. The right panels (b, d, and f) are magnified images as shown.

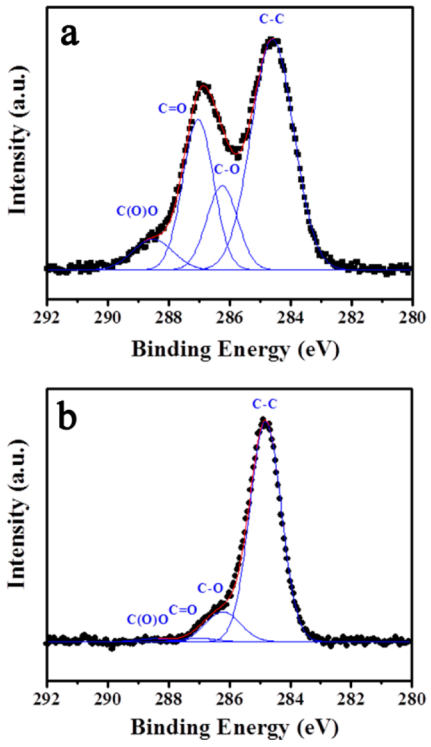

Figure 6. XPS spectra of (a) GO and (b) ERGO on the Au surface.

of the sp^2 domains and an increase in the number of new graphitic domains when GO is reduced.[16,32]

It is interesting to note that the intensities of the D and G bands are significantly enhanced after GO is reduced by the electrochemical process on the Au chip surface, in which 2D/D+G bands are also observed (Figure 7a). To investigate the reason for this enhancement, control experiments on ITO substrates are performed. As shown in Figure 7b, the D/G intensity ratios (I_D/I_G) of GO and ERGO on ITO substrates are 0.77 and 1.16, respectively, which indicates that GO are reduced, but no distinguishable SERS is observed on ITO substrates. The $I_{D(Au)}/I_{D(ITO)}$ and $I_{G(Au)}/I_{G(ITO)}$ ratios of GO are 1.50 and 1.35, respectively, indicating that a small enhancement of the GO Raman signal occurred on a Au chip surface (Table 2). When GO is reduced to ERGO, the Au substrate exhibits enormous enhancement to the Raman signal over the ITO substrate because $I_{D(Au)}/I_{D(ITO)}$ and $I_{G(Au)}/I_{G(ITO)}$ of ERGO are 6.20 and 5.91, respectively (as shown in Table 2). Therefore, the SERS of ERGO is mainly attributed to the Au substrate,

Table 2. Comparison of Graphene Raman Peaks (D and G) on Au and ITO Substrates

	$I_{D(Au)}/I_{D(ITO)}$	$I_{G(Au)}/I_{G(ITO)}$
GO	1.50	1.35
ERGO	6.20	5.91

from which both SPR phenomenon and metallic doping should be taken into account. It is well-known that SERS is mainly from the electromagnetic field excited by SPR on the Au surface, and this electromagnetic field is exponentially decayed with the increasing distance perpendicular to the Au surface.[58] Electrochemical reduction decreases the distance between carbon atoms and the Au surface by removal of the spacer of oxygen functional groups. This is supported by the results of the GO and ERGO thickness from SPR measurement in Table 1. The electromagnetic field is therefore exponentially enhanced, resulting in an enhancement of the ERGO Raman signal on the Au surface.

Another factor that should be considered is the metallic doping happening during electrochemical reduction. Parts a and b in Figure 7 show that the G band of ERGO shifts from 1595.4 cm^{-1} (on ITO) to 1596.7 cm^{-1} (on Au). The position of the 2D band shifts 16.6 cm^{-1} to a higher wavenumber. The I_{2D}/I_G intensity ratio is 0.22 on ITO, whereas it is 0.11 on Au. Furthermore, the G band is split into two distinct peaks on ERGO/Au in Figure 7c. This indicates that the Au film changes the electron density distribution in graphene and hence leads to phonon symmetry breaking at the Γ point (lifting degeneracy of LO and TO), which, in turn, splits the Raman G band (as shown in Figure 7c).[59,60] These results support that a p doping of ERGO occurred from the changes in the graphene electronic structure by the interaction between Au and ERGO.[59,60] The charge transfer from the doping effect of metal is also able to cause SERS on graphene.[59,60] The doping process could be reasonably explained by rearrangement of the gold atoms from a cyclic voltammetry treatment during electrochemical reduction.[61]

3.4. Application of SERS and DNA Binding. The assembled graphene substrates have been used for application of SERS detection of R6G and CV, as shown in Figure 8. The dye ethanol solution with the same concentration and volume is dripped onto substrates with identical area. SERS signals of the characteristic bands of R6G and CV can be clearly distinguished on Au-based substrates: ERGO/Au, GO/Au, and Au (the assignment of Raman bands is described in the SI). However, no visible Raman signal is observed on the ITO-

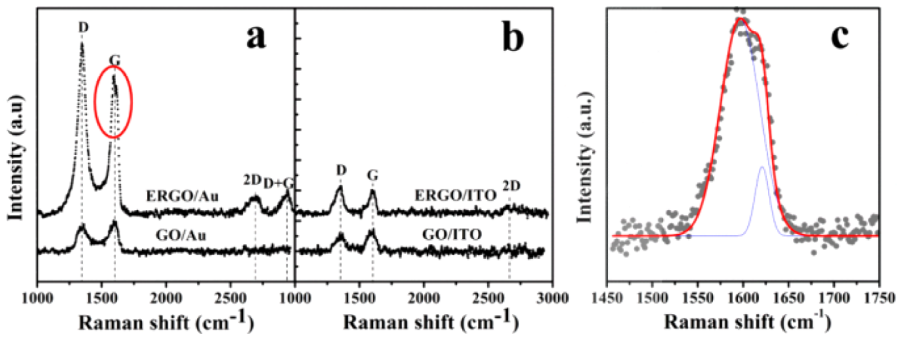

Figure 7. Raman spectra of GO and ERGO on a Au sensor chip (a) and on ITO substrate (b). (c) Deconvolved spectra of G bands of ERGO on a Au sensor chip.

dx.doi.org/10.1021/am400481t | ACS Appl. Mater. Interfaces 2013, 5, 2096−2103

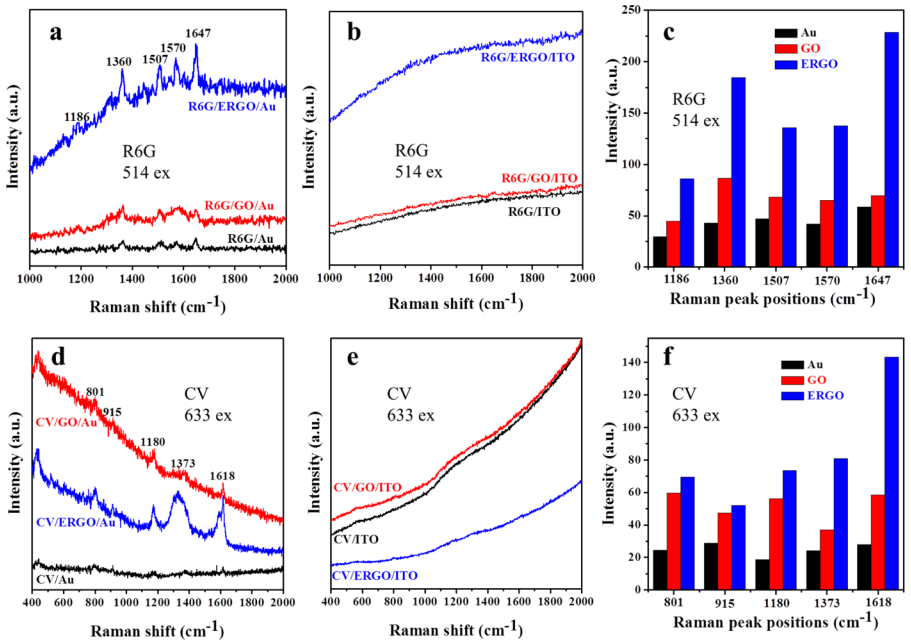

Figure 8. Raman spectra of 1×10^{-5} M R6G (a and b) and 1×10^{-5} M CV (d and e) dropped on a bare substrate (black line), GO (red line), and ERGO (blue line) on Au (a and d) and ITO (b and e) substrates. (c and f) Histograms of the SERS intensity of R6G and CV on Au, GO, and ERGO.

based substrates: ERGO/ITO, GO/ITO, and ITO. This phenomenon is consistent with the results of graphene Raman data in Figure 7, which confirms the electromagnetic field enhancement of R6G and CV molecules on Au substrates due to the SPR phenomenon.[62] Well-resolved spectral peaks are collected on the GO-modified Au film with a weak enhancement. This observation indicates that GO assembly indeed amplifies the SERS signals of R6G/CV molecules because of both effects of electromagnetic (SPR) and chemical mechanisms.[63,64] The SERS spectra on ERGO/Au are more intense, which is an expected result because the distance between graphene and the Au sensor chip decreases when GO is electrochemically reduced, similar to the results in Figure 7. The SERS enhancing effect of R6G and CV on the ERGO/Au substrate is visualized in the histograms in Figure 8c,f. Electrochemical reduction may also modify the electronic states and the Fermi energy level of GO that is able to enhance SERS.[16]

The interaction of DNA and GO is very important for a GO-based DNA quenching biosensor.[65] Taking advantage of the SPR technique, we investigated the difference of the binding abilities of single-stranded DNA (ssDNA) and double-stranded DNA (dsDNA) to GO and ERGO substrates (detailed SPR curves are shown in Figure S3 in the SI). The SPR responses of ssDNA/dsDNA binding to GO/ERGO are summarized by a bar graph in Figure 9. The results show that a higher response is always obtained from ssDNA than from dsDNA on both GO and ERGO surfaces. This is the first direct label-free evidence for the previous report that dsDNA interacts more weakly with graphene-based substrates than ssDNA due to $\pi-\pi$-stacking interaction.[66] In addition, the interaction of ssDNA/dsDNA to GO is stronger than that to ERGO substrates.[67] These results show that GO and ERGO substrates perform different interaction abilities with ssDNA and dsDNA, which is expected to be useful for the future design of a graphene-based DNA biosensor.

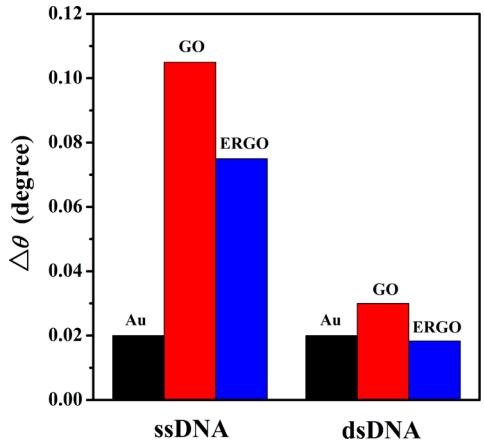

Figure 9. Change of SPR angles from ssDNA and dsDNA binding to Au, GO, and ERGO substrates.

4. CONCLUSIONS

A switch of the oxidation state of GO on a SPR chip for application of SERS and DNA−graphene interaction is investigated. The GO film is uniform and stable for electrochemical reduction. The thickness is reduced from 2.55 to 1.41 nm, and the real ($\varepsilon' = 1.62$) and imaginary ($\varepsilon'' = 0.01$) parts of the dielectric constant are increased to 7.41 and 2.26, respectively, when GO is electrochemically reduced. The ERGO/Au substrate exhibits significant enhancement for the Raman signal. We attribute this enhancement to the combined action of the doping effect and electromagnetic and chemical mechanisms. Application of these graphene-based substrates for SERS and the interaction of DNA with GO/ERGO are also illustrated. This work provides not only a new preparation approach and characterization method for the graphene film but also a new substrate for graphene-related research works on optoelectronics and biosensors.

dx.doi.org/10.1021/am400481t | ACS Appl. Mater. Interfaces 2013, 5, 2096−2103

■ ASSOCIATED CONTENT

Supporting Information

EIS, contact angles, SPR curves, and more SPR fitting results. This material is available free of charge via the Internet at http://pubs.acs.org.

■ AUTHOR INFORMATION

Corresponding Author

*E-mail: xqcui@jlu.edu.cn (X.C.), wtzheng@jlu.edu.cn (W.Z.).

Notes

The authors declare no competing financial interest.

■ ACKNOWLEDGMENTS

This work was financially supported by the National Natural Science Foundation of China (Grants 21075051, 21275064, and 50832001), the Program for New Century Excellent Talents in University (Project NCET-10-0433), and the "211" and "985" Projects of Jilin University, China, and State Key Laboratory of Electroanalytical Chemistry, CIAC, CAS.

■ REFERENCES

(1) Novoselov, K. S.; Geim, A. K.; Morozov, S. V.; Jiang, D.; Zhang, Y.; Dubonos, S. V.; Grigorieva, I. V.; Firsov, A. A. *Science* **2004**, *306*, 666−669.
(2) Schedin, F.; Geim, A. K.; Morozov, S. V.; Hill, E. W.; Blake, P.; Katsnelson, M. I.; Novoselov, K. S. *Nat. Mater.* **2007**, *6*, 652−655.
(3) Huang, X.; Qi, X. Y.; Boey, F.; Zhang, H. *Chem. Soc. Rev.* **2012**, *41*, 666−686.
(4) Cao, X.; Shi, Y.; Shi, W.; Lu, G.; Huang, X.; Yan, Q.; Zhang, Q.; Zhang, H. *Small* **2011**, *7*, 3163−3168.
(5) Dong, X. C.; Xu, H.; Wang, X. W.; Huang, Y. X.; Chan-Park, M. B.; Zhang, H.; Wang, L. H.; Huang, W.; Chen, P. *ACS Nano* **2012**, *6*, 3206−3213.
(6) Ramanathan, T.; Abdala, A. A.; Stankovich, S.; Dikin, D. A.; Herrera Alonso, M.; Piner, R. D.; Adamson, D. H.; Schniepp, H. C.; Chen, X.; Ruoff, R. S.; Nguyen, S. T.; Aksay, I. A.; Prud'Homme, R. K.; Brinson, L. C. *Nat. Nano* **2008**, *3*, 327−331.
(7) Huang, X.; Li, S. Z.; Huang, Y. Z.; Wu, S. X.; Zhou, X. Z.; Gan, C. L.; Boey, F.; Mirkin, C. A.; Zhang, H. *Nat. Commun.* **2011**, *2*, 292.
(8) Zeng, Z.; Huang, X.; Yin, Z.; Li, H.; Chen, Y.; Li, H.; Zhang, Q.; Ma, J.; Boey, F.; Zhang, H. *Adv. Mater.* **2012**, *24*, 4138−4142.
(9) Sun, X.; Liu, Z.; Welsher, K.; Robinson, J.; Goodwin, A.; Zaric, S.; Dai, H. *Nano Res.* **2008**, *1*, 203−212.
(10) Wang, L.; Pu, K.-Y.; Li, J.; Qi, X.; Li, H.; Zhang, H.; Fan, C.; Liu, B. *Adv. Mater.* **2011**, *23*, 4386−4391.
(11) He, Q. Y.; Sudibya, H. G.; Yin, Z. Y.; Wu, S. X.; Li, H.; Boey, F.; Huang, W.; Chen, P.; Zhang, H. *ACS Nano* **2010**, *4*, 3201−3208.
(12) Reina, A.; Jia, X.; Ho, J.; Nezich, D.; Son, H.; Bulovic, V.; Dresselhaus, M. S.; Kong, J. *Nano Lett.* **2008**, *9*, 30−35.
(13) Berger, C.; Song, Z.; Li, X.; Wu, X.; Brown, N.; Naud, C.; Mayou, D.; Li, T.; Hass, J.; Marchenkov, A. N.; Conrad, E. H.; First, P. N.; de Heer, W. A. *Science* **2006**, *312*, 1191−1196.
(14) Zhou, M.; Zhai, Y.; Dong, S. *Anal. Chem.* **2009**, *81*, 5603−5613.
(15) Guo, S.; Dong, S. *Chem. Soc. Rev.* **2011**, *40*, 2644−2672.
(16) Guo, H.-L.; Wang, X.-F.; Qian, Q.-Y.; Wang, F.-B.; Xia, X.-H. *ACS Nano* **2009**, *3*, 2653−2659.
(17) Wang, Z.; Zhang, J.; Chen, P.; Zhou, X.; Yang, Y.; Wu, S.; Niu, L.; Han, Y.; Wang, L.; Boey, F.; Zhang, Q.; Liedberg, B.; Zhang, H. *Biosens. Bioelectron.* **2011**, *26*, 3881−3886.
(18) Lin, L.; Liu, Y.; Zhao, X.; Li, J. *Anal. Chem.* **2011**, *83*, 8396−8402.
(19) Zhao, J.; Chen, G.; Zhang, W.; Li, P.; Wang, L.; Yue, Q.; Wang, H.; Dong, R.; Yan, X.; Liu, J. *Anal. Chem.* **2011**, *83*, 9100−9106.
(20) Ju, L.; Geng, B.; Horng, J.; Girit, C.; Martin, M.; Hao, Z.; Bechtel, H. A.; Liang, X.; Zettl, A.; Shen, Y. R.; Wang, F. *Nat. Nano* **2011**, *6*, 630−634.
(21) Liu, Y.; Cheng, R.; Liao, L.; Zhou, H.; Bai, J.; Liu, G.; Liu, L.; Huang, Y.; Duan, X. *Nat. Commun.* **2011**, *2*, 579.
(22) Watcharotone, S.; Dikin, D. A.; Stankovich, S.; Piner, R.; Jung, I.; Dommett, G. H. B.; Evmenenko, G.; Wu, S.-E.; Chen, S.-F.; Liu, C.-P.; Nguyen, S. T.; Ruoff, R. S. *Nano Lett.* **2007**, *7*, 1888−1892.
(23) Xu, Y.; Bai, H.; Lu, G.; Li, C.; Shi, G. *J. Am. Chem. Soc.* **2008**, *130*, 5856−5857.
(24) Salihoglu, O.; Balci, S.; Kocabas, C. *Appl. Phys. Lett.* **2012**, 100.
(25) Song, B.; Li, D.; Qi, W.; Elstner, M.; Fan, C.; Fang, H. *ChemPhysChem* **2010**, *11*, 585−589.
(26) Knoll, W. *Annu. Rev. Phys. Chem.* **1998**, *49*, 569−638.
(27) Bolduc, O. R.; Masson, J.-F. *Anal. Chem.* **2011**, *83*, 8057−8062.
(28) Guo, S.; Dong, S.; Wang, E. *ACS Nano* **2009**, *4*, 547−555.
(29) Paredes, J. I.; Villar-Rodil, S.; Solís-Fernández, P.; Martínez-Alonso, A.; Tascón, J. M. D. *Langmuir* **2009**, *25*, 5957−5968.
(30) Zhu, C.; Guo, S.; Fang, Y.; Dong, S. *ACS Nano* **2010**, *4*, 2429−2437.
(31) Tang, L.; Wang, Y.; Li, Y.; Feng, H.; Lu, J.; Li, J. *Adv. Funct. Mater.* **2009**, *19*, 2782−2789.
(32) Stankovich, S.; Dikin, D. A.; Piner, R. D.; Kohlhaas, K. A.; Kleinhammes, A.; Jia, Y.; Wu, Y.; Nguyen, S. T.; Ruoff, R. S. *Carbon* **2007**, *45*, 1558−1565.
(33) Hummers, W. S.; Offeman, R. E. *J. Am. Chem. Soc.* **1958**, *80*, 1339−1339.
(34) Cui, X.; Tawa, K.; Hori, H.; Nishii, J. *Adv. Funct. Mater.* **2010**, *20*, 546−553.
(35) Tawa, K.; Umetsu, M.; Hattori, T.; Kumagai, I. *Anal. Chem.* **2011**, *83*, 5944−5948.
(36) Cui, X.; Tawa, K.; Kintaka, K.; Nishii, J. *Adv. Funct. Mater.* **2010**, *20*, 945−950.
(37) Park, S.; Ruoff, R. S. *Nat. Nano* **2009**, *4*, 217−224.
(38) Hu, W.; Lu, Z.; Liu, Y.; Li, C. M. *Langmuir* **2010**, *26*, 8386−8391.
(39) Lukkari, J.; Salomäki, M.; Ääritalo, T.; Loikas, K.; Laiho, T.; Kankare, J. *Langmuir* **2002**, *18*, 8496−8502.
(40) Cui, X.; Sha, Y. F.; Yang, F.; Yu, P.; Li, J. N.; Yang, X. R. *Chin. J. Anal. Chem.* **2005**, *33*, 1639−1642.
(41) Damien, H. *Anal. Biochem.* **2001**, *288*, 109−125.
(42) Ekgasit, S.; Thammacharoen, C.; Knoll, W. *Anal. Chem.* **2003**, *76*, 561−568.
(43) Zhou, M.; Wang, Y.; Zhai, Y.; Zhai, J.; Ren, W.; Wang, F.; Dong, S. *Chem.—Eur. J.* **2009**, *15*, 6116−6120.
(44) Wang, Z.; Wu, S.; Zhang, J.; Chen, P.; Yang, G.; Zhou, X.; Zhang, Q.; Yan, Q.; Zhang, H. *Nanoscale Res. Lett.* **2012**, *7*, 1−7.
(45) Wang, Z.; Zhou, X.; Zhang, J.; Boey, F.; Zhang, H. *J. Phys. Chem. C* **2009**, *113*, 14071−14075.
(46) Yang, J.; Deng, S.; Lei, J.; Ju, H.; Gunasekaran, S. *Biosens. Bioelectron.* **2011**, *29*, 159−166.
(47) Wang, L.; Zhu, C.; Han, L.; Jin, L.; Zhou, M.; Dong, S. *Chem. Commun.* **2011**, *47*, 7794−7796.
(48) Cui, X.; Li, C. M.; Bao, H.; Zheng, X.; Zang, J.; Ooi, C. P.; Guo, J. *J. Phys. Chem. C* **2008**, *112*, 10730−10734.
(49) Zhu, C.; Fang, Y.; Wen, D.; Dong, S. *J. Mater. Chem.* **2011**, *21*, 16911−16917.
(50) Fan, X.; Peng, W.; Li, Y.; Li, X.; Wang, S.; Zhang, G.; Zhang, F. *Adv. Mater.* **2008**, *20*, 4490−4493.
(51) Nabok, A. V.; Tsargorodskaya, A.; Holloway, A.; Starodub, N. F.; Gojster, O. *Biosens. Bioelectron.* **2007**, *22*, 885−890.
(52) Damos, F. S.; Luz, R. C. S.; Kubota, L. T. *Electrochim. Acta* **2006**, *51*, 1304−1312.
(53) Félix, G.; Abdul-Kader, K.; Mahfoud, T.; Gural'skiy, I. y. A.; Nicolazzi, W.; Salmon, L.; Molnár, G.; Bousseksou, A. *J. Am. Chem. Soc.* **2011**, *133*, 15342−15345.
(54) Yang, D.; Velamakanni, A.; Bozoklu, G.; Park, S.; Stoller, M.; Piner, R. D.; Stankovich, S.; Jung, I.; Field, D. A.; Ventrice, C. A., Jr.; Ruoff, R. S. *Carbon* **2009**, *47*, 145−152.
(55) Shin, H.-J.; Kim, K. K.; Benayad, A.; Yoon, S.-M.; Park, H. K.; Jung, I.-S.; Jin, M. H.; Jeong, H.-K.; Kim, J. M.; Choi, J.-Y.; Lee, Y. H. *Adv. Funct. Mater.* **2009**, *19*, 1987−1992.

(56) Eda, G.; Fanchini, G.; Chhowalla, M. *Nat. Nano* **2008**, *3*, 270−274.
(57) Ferrari, A. C.; Robertson, J. *Phys. Rev. B* **2000**, *61*, 14095−14107.
(58) Lal, S.; Grady, N. K.; Kundu, J.; Levin, C. S.; Lassiter, J. B.; Halas, N. J. *Chem. Soc. Rev.* **2008**, *37*, 898−911.
(59) Lee, J.; Novoselov, K. S.; Shin, H. S. *ACS Nano* **2010**, *5*, 608−612.
(60) Dong, X.; Shi, Y.; Zhao, Y.; Chen, D.; Ye, J.; Yao, Y.; Gao, F.; Ni, Z.; Yu, T.; Shen, Z.; Huang, Y.; Chen, P.; Li, L.-J. *Phys. Rev. Lett.* **2009**, *102*, 135501.
(61) Jin, Y.; Dong, S. *J. Phys. Chem. B* **2003**, *107*, 13969−13975.
(62) Fathima, S. J. H.; Paul, J.; Valiyaveettil, S. *Small* **2010**, *6*, 2443−2447.
(63) Yu, X.; Cai, H.; Zhang, W.; Li, X.; Pan, N.; Luo, Y.; Wang, X.; Hou, J. G. *ACS Nano* **2011**, *5*, 952−958.
(64) Chen, P.; Yin, Z.; Huang, X.; Wu, S.; Liedberg, B.; Zhang, H. *J. Phys. Chem. C* **2011**, *115*, 24080−24084.
(65) He, S.; Song, B.; Li, D.; Zhu, C.; Qi, W.; Wen, Y.; Wang, L.; Song, S.; Fang, H.; Fan, C. *Adv. Funct. Mater.* **2010**, *20*, 453−459.
(66) Tang, L. H.; Chang, H. X.; Liu, Y.; Li, J. H. *Adv. Funct. Mater.* **2012**, *22*, 3083−3088.
(67) Pei, H.; Li, J.; Lv, M.; Wang, J. Y.; Gao, J. M.; Lu, J. X.; Li, Y. P.; Huang, Q.; Hu, J.; Fan, C. H. *J. Am. Chem. Soc.* **2012**, *134*, 13843−13849.
(68) Jung, I.; Vaupel, M.; Pelton, M.; Piner, R.; Dikin, D. A.; Stankovich, S.; An, J.; Ruoff, R. S. *J. Phys. Chem. C* **2008**, *112*, 8499−8506.
(69) Bruna, M.; Borini, S. *Appl. Phys. Lett.* **2009**, *94*, 031901−031903.